A new smog chamber system for atmospheric multiphase chemistry study: design and characterization

Taomou Zong[1], Zhijun Wu[1,2,*], Junrui Wang[1,3], Kai Bi[4], Wenxu Fang[1], Yanrong Yang[1], Xuena Yu[1], Zhier Bao[5], Xiangxinyue Meng[1], Yuheng Zhang[1], Song Guo[1,2], Yang Chen[5], Chunshan Liu[6], Yue Zhang[7], Shao-Meng Li[1], Min Hu[1,2]

[1]State Key Joint Laboratory of Environmental Simulation and Pollution Control, College of Environmental Sciences and Engineering, Peking University, Beijing 100871, China

[2]Collaborative Innovation Center of Atmospheric Environment and Equipment Technology, Nanjing University of Information Science and Technology, Nanjing 210044, China

[3]Laboratory of Atmospheric Observation Supersite, School of Environment and Energy, Peking University Shenzhen Graduate School, Shenzhen 518055, China

[4]Beijing Key Laboratory of Cloud, Precipitation and Atmospheric Water Resources, Beijing, 100089, China

[5]Research Center for Atmospheric Environment, Chongqing Institute of Green and Intelligent Technology, Chinese Academy of Sciences, Chongqing, 400714, China

[6]Beijing Convenient Environmental Tech Co. Ltd., Beijing 101115, China

[7]Department of Atmospheric Sciences, Texas A&M University, College Station, TX 77843, United States

Correspondence to: Zhijun Wu (zhijunwu@pku.edu.cn)

E-mail lists:

Taomou Zong (zongtaomou@pku.edu.cn)
Zhijun Wu (zhijunwu@pku.edu.cn)
Junrui Wang (18845725921@163.com)
Kai Bi (bikai_picard@vip.sina.com)
Wenxu Fang (343299989@qq.com)
Yanrong Yang (yyr2020@stu.pku.edu.cn)
Xuena Yu (99784925@qq.com)
Zhier Bao (baozhier@cigit.ac.cn)
Xiangxinyue Meng (mxxy96@126.com)
Yuheng Zhang (zhangyh@stu.pku.edu.cn)
Song Guo (guosong@pku.edu.cn)
Yang Chen (chenyang@cigit.ac.cn)
Chunshan Liu (bjkwnt@163.com)
Yue Zhang (Yuezhang@tamu.edu)
Shao-Meng Li (shaomeng.li@pku.edu.cn)
Min Hu (minhu@pku.edu.cn)

Abstract. Multiphase chemistry is an important pathway for the formation of secondary organic aerosols in the atmosphere. In this study, an indoor 2 m^3 Teflon chamber system (Aerosol multIphase chemistry Research chamber, AIR) was developed and characterized to specifically simulate atmospheric multiphase chemistry processes. The temperature and humidity controls, diurnal variation simulation, and seed particle generation unit in this chamber system were designed to meet the needs of simulating multiphase atmospheric chemical reactions. The AIR chamber is able to accurately control temperature (2.5 ~ 31 ± 0.15 ℃) and relative humidity (RH < 2 % ~ > 95% ± 0.75%) over a relatively broad range. In addition, an RH regulation module inside the chamber was designed to simulate the diurnal variation of ambient atmospheric RH. The aerosol generation unit is able to generate pre-deliquescent seed particles with an organic coating across a wide range of phase states or morphologies. The organic coating thickness of the aerosols within the chamber can be precisely controlled through adjusting the condensation temperature, further helping to elucidate the roles of seed particles in multiphase chemical reactions. The inner walls of the AIR chamber are passivated to reduce the wall loss rates of reactive gases. Yield experiments of α-pinene ozonolysis with and without seed particles combined with a box model simulation demonstrate the high-quality performance of secondary aerosol formation simulation using the AIR chamber.

1 Introduction

Smog chamber is a mainstream tool in chemical laboratory studies to simulate the formation and evolution of air pollutants (Batchvarova et al., 2006; Chen and Lelevkin, 2006; Kolev and Grigorieva, 2006; Mocanu et al., 2006; Tolkacheva, 2006) and reveal the parameterization or mechanisms of atmospheric processes (Wenger, 2006; Olariu et al., 2006; Bejan et al., 2006; Mellouki, 2006; Barnes, 2006; Albu et al., 2006; Carter, 2006; Rudzinski, 2006; Zielinska et al., 2006). Chamber simulations have irreplaceable advantages over other laboratory methods such as oxidation flow reactors (Kang et al., 2007; Lambe et al., 2015; Corral Arroyo et al., 2018; Cosman and Bertram, 2008) and bulk solution experiments (Brunamonti et al., 2015; Turšič et al., 2003; Pratap et al., 2021; Fleming et al., 2020; Mekic et al., 2019) in tracking atmospheric transformation processes and understanding kinetic processes.

The development of chambers is closely related to advances in atmospheric chemistry research. Starting with studies of photochemical smog in Los Angeles in the 1940s (Haagensmit, 1952) and continuing to the 1970s, chambers were designed primarily to study the formation of ozone (Akimoto et al., 1979; Carter et al., 1982) as well as the chemistry of volatile organic compounds (VOCs) and NO_x (Morriss et al., 1957) in the atmospheric boundary layer. With the development of submicron particle measurement techniques, chambers were further used in secondary organic aerosol (SOA) formation studies from the 1980s leading to numerous important scientific discoveries (Hidy, 2019; Odum et al., 1996; Odum et al., 1997; Griffin et al., 1999; Paulsen et al., 2005; Rollins et al., 2009; Hu et al., 2014; Wang et al., 2014).

Since the beginning of the 21st century, many chambers have been built or upgraded to address integrated atmospheric scientific questions, including $PM_{2.5}$ pollution (Johnson et al., 2004; Hallquist et al., 2009; Hurley et al., 2001), reaction kinetic parameters, mechanisms of VOC oxidation intermediates (Brauers et al., 2003; Bohn et al., 2004; Ren et al., 2017), as well as multiphase processes (Warneke and C., 2004; Pöschl and Shiraiwa, 2015; Liu and Abbatt, 2021; Franco et al., 2021).

In recent years, multiphase chemistries have been invoked to explain the bursting growth of particles (Su et al., 2016; Wang et al., 2016; Su et al., 2020) and physicochemical processes of SOA formation under high ion strength conditions in the atmosphere (Cheng et al., 2015; Su et al., 2020; Liu et al., 2021). Atmospheric multiphase processes can undergo different reaction pathways that are influenced by different environmental conditions (e.g., light, temperature, and relative humidity (RH)) and aerosol physicochemical properties including aerosol liquid water content (ALWC), aerosol phase state, and morphology (George and Abbatt, 2010; Davidovits et al., 2011; Abbatt et al., 2012; Ziemann and Atkinson, 2012; Herrmann et al., 2015; Ravishankara, 1997; George et al., 2015; Su et al., 2020). Thus, a precise control of such parameters in a chamber system is vital for simulating atmospheric multiphase chemistry. Different from outdoor chambers (Leone et al., 2010; Stern et al., 1987; Pandis et al., 1991; Johnson et al., 2004; Martin-Reviejo and Wirtz, 2005; Rollins et al., 2009; Cocker et al., 2001; Peng et al., 2017), indoor chambers are usually equipped with artificial light sources (Takekawa et al., 2003; Carter et al., 2005; Paulsen et al., 2005), that can provide controllable irradiation for the simulation of multiphase processes. Compared to large chambers (Brauers et al., 2003; Leone et al., 1985; Pandis et al., 1991), temperature and RH inside small chambers can achieve faster equilibria and provide a more precise simulation of parameters such as diurnal RH change and ALWC (Takekawa et al., 2003; Carter et al., 2005; Paulsen et al., 2005; Wang et al., 2014; Bin Babar et al., 2016), thus improving reproducibility and efficiency when conducting experiments. In addition, small chambers may have the potential for controlling RH change and simulating co-condensation phenomena. Adversely, the wall loss effects are more significant for small chambers (Carter et al., 1982; Carter and Lurmann, 1991; Dodge, 2000). The influence of aerosol phase state on kinetics of gas-particle interactions has received increasing attention (Virtanen et al., 2010; Berkemeier et al., 2016; Wang et al., 2015a; Reid et al., 2018), and this requires the phase state of seed particles can be controlled in chamber simulations. A laboratory study using pre-deliquescence way to control particle phase state has been reported (Faust et al., 2017), providing a feasible way for phase state control. In regard of particle morphology, some chamber-based

experimental studies in recent years have preliminarily shown that organic coatings have important effects on the kinetics of aerosol multiphase transformation (Zhou et al., 2019; Zhang et al., 2018; Zhang et al., 2019), which deserves more researches. As these studies showed evidence that the morphology and phase state of aerosol particles play important roles in the atmospheric multiphase chemistry processes, focused chamber studies on multiphase chemistry require additional steps to control the morphology and phase state of seed particles in chamber design.

In this study, we designed and built a new indoor 2 m^3 Teflon chamber system (Aerosol multIphase process Research chamber, AIR) with a focus on accurately simulating atmospheric multiphase processes. The temperature and RH inside the AIR chamber were precisely controlled to within ± 0.15 ℃ and ± 0.75 %, respectively. A quantitative manipulation of the RH cycle was designed to simulate the diurnal variations in ambient RH. The seed generation subsystem, including an inorganic particle pre-deliquescence unit and an organic-coating unit, was designed to manipulate the aerosol phase state and organic-coated morphology. A series of experiments were conducted to characterize the spectral distribution and photolysis parameters of light sources, temperature, RH, wall loss behaviors of gas and particles, and particle morphology. Additionally, a series of experiments involving the oxidation of α-pinene with seed particles were conducted in the AIR chamber to demonstrate the effectiveness of the chamber in simulating atmospheric multiphase chemistry. Our results indicate that the AIR chamber system has more precise temperature and RH control capabilities compared to other chambers. Phase state and morphology of seed particles can also be accurately manipulated in advance, which is rare in existing smog chamber systems.

2 Facility

Figure 1 displays the schematic design of AIR chamber system, and the real picture of the reactor bag and enclosure system are shown in Fig. S1. The chamber system includes the 2 m^3 fluorinated ethylene propylene (FEP) Teflon film (75 μm, Du Pont, USA, light transmission ≥ 93%) reactor and the associated temperature and RH control, artificial light sources, zero air injection and humidification, gaseous/liquid precursor injection, seed aerosol generation, and the instrument-optional detection components. To achieve a precise control of thermodynamic parameters and aerosol morphology when simulating atmospheric multiphase chemistry processes, the temperature inside the reactor is precisely controlled to

within ± 0.15 ℃. An RH regulation module is designed and built to simulate the ambient RH diurnal variation, which is capable of changing the RH in the reactor at a time scale of half an hour. In addition, a pre-deliquescing device and a coating device are custom-built to couple to the seed aerosol generation component, for manipulating the phase state (metastable aqueous or solid) and core-shell morphology (1 % ~ 12 % shell thickness) of seed aerosols. The detailed description of each system is shown in Section 2.1-2.4.

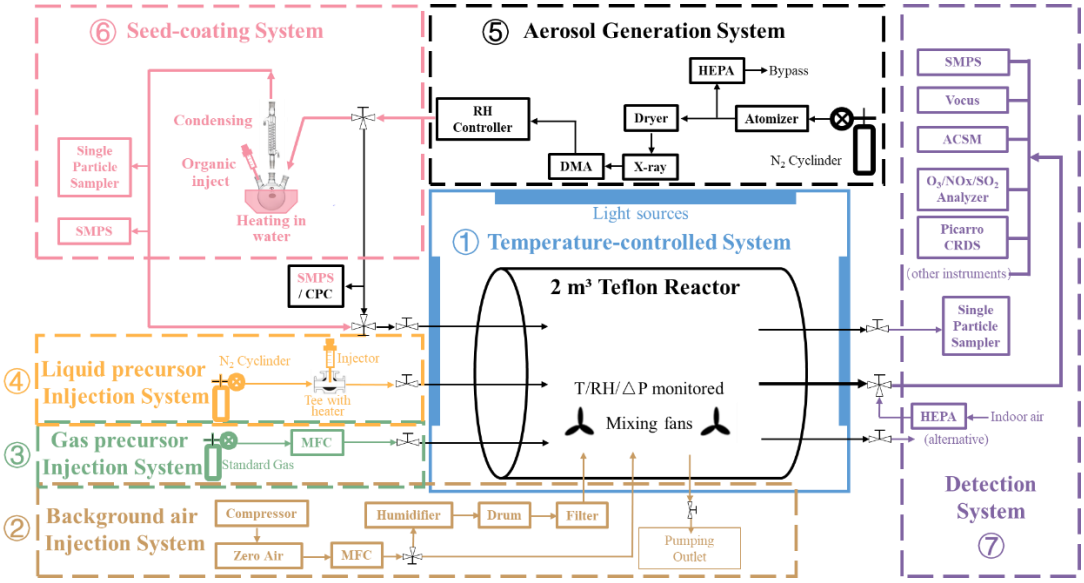

Figure 1. Schematic diagram of AIR chamber system.

2.1 The reactor and enclosure

The Teflon reactor is a 2 m^3 horizontal cylinder (1.2 m in diameter, 1.8 m in length). It is fixed on a stainless-steel frame with four ridges firmly adhered on the Teflon air bag (Fig. S1), so that the variable volume of the reactor during sampling is adequate (this chamber system is designed to operate in Batch Mode). As to each circle side of the cylinder, three stainless steel tubes are threaded through the Teflon film to act as the inlets (for injecting seeds and liquid phase precursors) or sampling outlets for the detection system, respectively. The interface between each tube and the film is sealed by a Teflon flange and a perfluorinated O-ring. At the bottom inside the reactor, two magnetic-levitation fans (patent number: 2019213329392, Beijing Convenient Environmental Tech Co. Ltd.) are equipped, with four speed levels (1000, 1350, 1700, 2000 rpm). A temperature and RH sensor (HMP110, Vaisala, Finland) and a differential pressure sensor (MSX-W10-PA-LCD, Dwyer, America) are also equipped at the bottom inside the reactor.

The rectangular enclosure (2.4 × 1.6 × 2.3 m, L, W, H) of the reactor is temperature-controlled by a

circulation system. The indoor air is introduced from the top of the enclosure and exhausts through the bottom. The chiller power is constant, while the heating power is controlled through a proportional-integral-derivative (PID) feedback. Forty black lights (1.2 m, 40 W, Bulb-T12, GE, USA) are fixed on the inner wall of the enclosure as light sources for atmospheric process simulation. The number and position of these lights in work can be controlled by the system computer, so that the light intensity can be variable in experiments. Specular insulated material (SUS304, stainless steel, 8K, mirror plate) is used as the enclosure inner wall so that the irradiation inside the reactor can be homogeneous. One side of the enclosure is a double door for entering and reactor maintenance.

2.2 Cleaning and humidifying system

The background gas in the reactor is from the indoor air. An air compressor (FOHUR, FH-50L) compresses the indoor air into a zero-air generator (Aadco, 737-14-A-CH4-240) for purification, removing airborne contaminants such as particulate matters, hydrocarbons, water vapor, NOx, O_3 and SO_2 to produce zero air (RH can be dried to < 2%, and the background concentrations of other contaminants are displayed in Table S2). Then, with the control of a mass flow controller (MFC, HORIBAMETRON, S4832/HMT), zero air is fed into the reactor through a 1/2" stainless steel tube (sealed at the bottom interface by a 304 stainless steel flange) at a flow rate of ≤ 50 L/min (to ensure the cleaning efficiency of the zero-air generator is sufficient), acting as the background gas and cleaning gas for the reactor. At the same time of feeding into the cleaning zero air, a pump beside the chamber system will exhaust the air from the reactor with a flow rate of 20 L/min to accelerate the gas exchange. The positive differential pressure inside the reactor is monitored. When the differential pressure reaches 30 Pa, the MFC will stop the zero-air feed, and when the value falls below 20 Pa, zero air feed will restart. This is designed to avoid damaging the Teflon film of the reactor during cleaning.

The zero air is also used as humidifying gas. When switching to the humidification mode, the zero air will go into a humidification tank filled with deionized water (Milli-Q, 18MΩ) switched by a three-way valve, generating humidified zero air. Then, the humidified air flows through a filter (Waterman, HEPA) to remove the water droplet, and injects into the reactor to humidify. During the humidifying, the exhaust pump mentioned above keeps working. The flow rate of the humidified zero air (20 ~ 25 L/min) is set to be slightly higher than the exhausting rate for fast reaching the target RH inside the reactor.

2.3 Precursor injection system

According to the phase state of precursor reagents, the precursor injection system of this chamber system contains two types. One is used for the injection of gaseous precursors. Standard gas cylinders containing reactive gas (such as SO_2, NO_2, NH_3, HCHO, etc.), inject relevant gaseous precursors into the reactor at a set flow rate and injecting duration under the control of a computer-connected MFC. The oxidant O_3 is produced through the decomposition of O_2 (from a standard O_2 cylinder) exposed to the 185 nm UV light. After flowing through the MFC, the gaseous species enter the reactor via a stainless-steel tube at the bottom of the chamber.

The other type is used for the injection of liquid precursors. Note that, the liquid precursors here mean the species is in liquid phase before injected into the reactor, but should be gaseous after injecting into the chamber, such as α-pinene standard solvent. A tee (the inlet on the left side of the chamber, as shown in the 'Liquid precursor Injection System' in Fig. 1) is fitted in the pipeline before the liquid precursors entering the reactor, with a 1 mm thick silicone membrane clamped to the right-angled end. The specific amount of the liquid precursors is taken with a microsyringe, penetrating the silicone membrane and slowly injected into the tee. At the same time, pure N_2 is used as the carrier gas to vaporize the liquid precursor and carry it into the reactor under a specific gas cylinder pressure (0.25 MPa). After injection, N_2 is continuously purged for 60 seconds to ensure that no liquid precursors remain in the pipeline.

2.4 Seed generation system

The seed aerosol generating system is a complex subsystem of AIR chamber system designed in this study. In addition to the common aerosol generation device, this study couples an RH-controlling device and a coating device to control the phase state and morphology of the seeds for supporting the simulation of atmospheric multiphase processes.

Commonly, the species used to generate the seed particles (typically dissolved inorganic salts such as ammonium sulfate and sodium chloride) are first dissolved in deionized water (Milli-Q, 18 MΩ) and then generate a solution. Then, it is atomized as humid aerosol flow by an atomizer (TSI 3076) with N_2 blowing. Passing through a Nafion tube (PERMA PURE, MD-700-24F-3), the humid flow is dried and forms dry polydisperse seed aerosols. The drying is realized by pumping the air at the outer layer of the Nafion tube to a negative pressure (~20 kPa). It is tested that, within the range of the aerosol generation flow rate (≤ 3 L/min), the RH of the aerosol flow can be dried to below 30 %. An X-ray neutralizer and

DMA (DMA, Model 3082, TSI, Inc., USA) are optional, for selecting monodisperse aerosols from the polydisperse aerosol flow (flow rate ratio of sheath flow to aerosol flow is controlled between 5:1 and 10:1), to support monodisperse experiments. For polydisperse seeds experiments, the seed generation system can inject seeds into the reactor to the desired amount within a time scale of seconds to several minutes. For monodisperse seeds experiments, if large-sized seeds that have a lower number fraction in the generated aerosol population are selected, the time scale will expand to 40-50 minutes. The appropriate time scale for seed injection can be adjusted by changing the solution concentration and aerosol flow rate.

Besides, an RH controlling device is designed in this study to pre-deliquesce the generated dry seeds that forming metastable seed aerosols. As shown in Fig. S9, N_2 is used as the initial gas, which is then divided into two paths, one is the dry N_2, and the other goes through the deionized water (Milli-Q, 18MΩ, heated to 45 ℃) to act as the wet gas. The flow rate of each path is controlled by an MFC (GAS TOOL INSTRUMENT, GT 130MAX). Then the two flows mix into one as the humidifying gas and enter the outer layer of a Nafion semi-permeable tube (PERMA PURE, MD-700-24F-3). The flow with seed aerosols goes through the inner layer of the Nafion tube and then is humidified. The RH of the humidified flow is detected by an RH sensor (HYGROCLIP2, HC2A-S). The two MFCs of each flow path and the RH sensor are connected to a computer and controlled by a Labview program with PID feedback. Through the two MFCs adjusting the ratio of the flow rates of the dry and wet flow path, the RH of seed aerosol flow is controlled. This device has been tested to enable rapid changes in RH between 5 % and 90% within 5 mins, and the RH variability can be within ± 0.2 %.

In order to investigate the effect of aerosol coating on atmospheric multiphase process, a device is designed in this study to generate a thickness-controlled and species-known coating on the generated dry monodisperse seed aerosols. The constitution of the coating device is shown in Fig. S10. This device consists of a water bath (Changfeng, HW.SY11-KP1), a three-necked flask (250 mL, 19#-24#-19#), a condensing glass tube (30 cm, 24#), and a thermostatic bath (BiLon, SC-05B). The organic species (~ 400 μL) with low volatility (saturated vapor pressure in the order of 10^{-4} ~ 10^{-5} mmHg at room temperature) used to form coating is set at the bottom of the three-necked flask, which is heated in the water bath to evaporate the organic vapor. The dried seed aerosol flow enters through the side port of the three-necked flask, and then carries the hot organic vapor into the condensing tube (condensing temperature is controlled at 20 ℃ by the thermostatic bath in this study). Due to the reduced temperature,

239 the saturated vapor pressure of the organic drops, and the organic vapor will preferentially condense on
240 the surface of seed aerosols that forming a coating. The coating efficiency can keep stable within four
241 hours, which is sufficient to meet the duration of injecting seeds for general experiments.

242 **2.5 Detection system**

243 As shown in Figure 1, three stainless steel tubes are fixed on the right side of the reactor to act as sampling
244 outlets. The middle steel tube of them is 3/8 " in size and acts as the main sampling tube, connected to a
245 3/8 " stainless steel three-way plug valve. One outlet of the plug is attached to a HEPA filter, and the
246 other outlet is attached to the line to sampling instruments. This design allows a quick sampling switch
247 between indoor air and the reactor. The other two stainless steel tubes are both 1/4 " and are used as
248 auxiliary sampling outlets (e.g. temporarily collect single particle samples for a few minutes).
249 An SMPS system (a DMA, Model 3082, and a CPC, Model 3772, TSI, Inc., USA), and a CPC (Model
250 3750, TSI, Inc., USA) downstream of the seed generation system, are the standing instruments for the
251 chamber system, used to measure the particle number size spectrum distribution and particle total number
252 concentration in the reactor, respectively. Other instruments are optional according to the specific
253 research aim, and typically the total sampling flow rate should be lower than 6 L/min.
254 The other detection instruments involved in this study, include the instruments for gaseous species
255 detection (Thermo Scientific gas analyzer (Model 43i-TLE for SO_2, Model 42i-TL for NOx, Model 49i
256 for O_3, Model 48i-TLE for CO), Picarro cavity ring-down spectroscopy (Picarro CRDS, G2401) for CO_2
257 and CH_4, Summa Canister (SILONITE, 1869) and GC-MS (Agilent, 7890A/5975C) for non-methane
258 hydrocarbon (NMHC)), instruments for particulate species detection (Time-of-Flight Aerosol Chemical
259 Speciation Monitor (ToF-ACSM, Aerodyne)), and instruments for volatile organic compounds (Vocus
260 Proton-Transfer Reaction Time-Of-Flight Mass Spectrometry (Vocus-PTR-TOF-MS, Vocus S, Tofwerk),
261 shorted as Vocus).
262 The sampling flow rate of each instrument is calibrated before each experiment. For Thermo Scientific
263 instruments and Vocus, a single standard concentration is tested at each experiment, to act as a basis for
264 instruments status verification and data quantification. For the data collected by ACSM, the calibration
265 is performed based on the mass concentration calculated from SMPS data.

3 Characterization of the AIR chamber

A series of experiments were carried out to evaluate the performance of this chamber system, including leakproofness, sample-volume support, background concentrations, mixing performance, light characteristics, temperature and RH control, gas and particle wall loss, as well as characterizations of aerosol particles with the core-shell morphology. All the instruments for measurement are included in Section 2.5.

3.1 Fundamental parameters

Leakproofness of the reactor was characterized by the positive pressure difference between the air inside the reactor and the ambient air and the change in the total number concentration of background particles inside the reactor. When the reactor was filled with zero air, the positive pressure difference inside the reactor was maintained at > 3 Pa within 24 hours (Fig. S2a), then slowly decreased to ~ 0.5 Pa after several days. When the air inside the reactor was sampled at a flow rate of 5 L/min, the positive pressure difference decreased to zero after 2 hours, and then total particle number concentration slowly increased from ~ 0 cm^{-3} to a final < 10 cm^{-3} in ~3.5 hours (Fig. S2b). This concentration is negligible for a particle number concentration of 10^3 ~ 10^4 cm^{-3} that are usually used in experiments. Moreover, this chamber system is designed to operate in batch mode, and the reactor can provide a sampling volume of 1000 ~ 1200 L (Fig. S3) and a sampling time of more than 3 hours at a total sampling flow rate of 5~6 L/min. The results above indicate that the system leakproofness is reliable for further experiments.

The reactor background was also characterized after repeated cleaning with zero air. As shown in Fig. S4, the background particle total number concentration was < 1 cm^{-3}, and increased only to 4 cm^{-3} with the mixing fans turned on. Irradiation slightly increased the background particle concentration but still only to < 10 cm^{-3}, which is negligible when compared with normal reaction conditions. Table S1 shows the background concentrations of chemical species in AIR chamber reactor under dry and high RH conditions. Compared with data reported for other chambers (White et al., 2018; Bin Babar et al., 2016; Wang et al., 2014; Platt et al., 2013; Carter et al., 2005; Chen et al., 2019b), the background concentrations of gaseous pollutants including SO_2, NOx, O_3 and CO in the reactor were comparable or lower for the AIR chamber. The background concentration of total non-methane hydrocarbon (NMHC) was higher than literature values due to the presence of chemically inert $CHClF_2$ (half of the total NMHC concentration), which originates from the indoor refrigeration system and is hard to eliminate within the

zero-air generation system. Nevertheless, this species does not interfere with the reactions under most experimental conditions. The reactor can be cleaned to background levels with a volume of zero air >5 times that of the reactor (Table S2) after each experiment. The cleaning process can be completed in less than 9 hours, as shown in Section 2.2.

The mixing performance of the injection into the reactor was examined using NO_2 concentration and total particle number concentration as tracers (Fig. S5). The mixing time to uniformity (the duration between the two plateaus in Fig. S5) was 5 minutes without running fans and less than 1 minute with the fans on. Furthermore, the mixing time was independent of the fan speed.

3.2 Light source characterization

The reflective inner wall (SUS304, stainless steel, 8K, mirror plate) of the AIR chamber is equipped with 40 UV lamps (1.2 m, 40 W, Bulb-T12, GE, USA) to provide irradiation during the experiments. There are 10 lamps on the left, right, back, and top of the wall, respectively, and each lamp can be turned on or off separately by the control system, so that the light intensity in experiments varies from 2.5% to 100% intensity. These light sources can also be replaced by lamps with different emission spectra to provide a variety of irradiation conditions.

For current light sources, a portable UV spectrometer (StellarNet Inc., Tampa FL, USA) was used to characterize the irradiance spectrum in the reactor (Fig. S6). The irradiance is mainly distributed in the range of 360 ~ 390 nm, peaking at 370 nm, which is within the range of peak irradiance of UV lights used in other indoor chambers (340 ~ 371 nm) (Wang et al., 2014; Ma et al., 2022; Bin Babar et al., 2016; Chen et al., 2019b; Lane and Tang, 1994; Thuner et al., 2004). Another small peak appears at 405 nm, which is convenient for directly checking the status of the lamps.

The photolytic rate constant for NO_2 can be used to characterize the irradiation intensity. Previous literature (Wang et al., 2014; Bin Babar et al., 2016; Ma et al., 2022) often characterize irradiation intensity through the photolytic rate constant of NO_2 (J_NO_2), calculated through the steady-state concentrations of NOx and O_3 (Atkinson et al., 2004). This study mainly used a spectrometer, namely the Jvalue instrument (AVANTES, AvaSpec-ULS-TEC-EVO), to measure the irradiance and directly calculate the photolytic rate constants of a few important species in atmospheric photochemistry. Notably, the Jvalue instrument was also calibrated using the J_NO_2 values derived from the steady NOx-O_3 concentration under several light schemes to correct for the geometry defect of the Jvalue instrument

when placed inside the AIR chamber. The calibration factor of the traditional J_NO_2 method is 1.49 ± 0.06. As shown in Table S3, the current light source is more suitable for the photolysis of HONO and NO_2 (photolytic rate constants on the order of $10^{-4} \sim 10^{-3}$ s^{-1}). However, the photolysis of HCHO, H_2O_2, and O_3 is slow (photolytic rate constants on the order of 10^{-8}~10^{-7} s^{-1}). The J_NO_2 maxima of other chambers are usually in the range of $2 \sim 9 \times 10^{-3}$ s^{-1} (Chen et al., 2019a; Li et al., 2017; Wang et al., 2014; Bin Babar et al., 2016; Ma et al., 2022). In comparison, J_NO_2 due to the light source in the AIR chamber is 4.10×10^{-3} s^{-1}, close to the median value of the other chambers. Moreover, the photolytic rate constant of HONO due to the light source in this chamber (J_HONO at the level of 10^{-4} s^{-1}) is comparable to or slightly higher than the value of HONO photolysis in the ambient atmosphere in China (J_HONO at the level of $10^{-5} \sim 10^{-4}$ s^{-1}) (Zheng et al., 2020).

When only lamps on two sides of the AIR chamber were turned on (four schemes with 20 lights on, noted as 'only back/top', 'left and right', 'odd' and 'even' in Table S3), the photolytic rate constants in the reactor under different configurations were almost the same (J_HONO = $5.10 \pm 0.12 \times 10^{-4}$ s^{-1}, J_NO_2 = $2.16 \pm 0.05 \times 10^{-3}$ s^{-1}), and nearly equal to half of that with all 40 lights on. In addition, the photolytic rate constant of the scheme 'left and right' (20 lights) was the sum of that of 'only left' (10 lights) and 'only right' (10 lights). These results indicate that the irradiation in the reactor is uniformly distributed. Notably, because the measurement interface of Jvalue was a little biased to the left during detection, the value for 'only left' was higher than that for 'only right'.

3.3 Performance of temperature and RH control

The temperature and RH in the reactor are measured by a high-accuracy sensor (HMP110, Vaisala, Finland). Detailed descriptions of temperature and RH control are given in Section 2.1 and 2.2. The internal design of our chamber enclosure ensures that the circulating air, which controls the temperature surrounding the reactor, reaches equilibrium (taking < 2 hours as shown in Fig. 2) from the outside of the Teflon film to the inside. This design guarantees that the temperature distribution is spatially homogeneous, even for a chamber system with a 30 m^3 reactor (Wang et al., 2014). The accuracy for RH of this sensor is shown by its measurement error of < 1% from that measured by a hygrometer (chilled mirror hygrometer, Edgetech Instrument, USA), with an $R^2 > 0.99$. The temperature in the reactor can be stably controlled in the range of 2.5 ℃ ~ 31 ℃, and the control range of RH is < 2% ~ > 95%. The fluctuations in the temperature inside the reactor are within ± 0.15 ℃ of any set temperature, and the

corresponding RH fluctuations for RH > 80 % are within ± 0.75 %. The RH fluctuation caused by the water permeation through the FEP filter can be ignored due to the slow permeation rate of water molecules (0.007L/m^2/24h/atm). The stability achieved with the temperature and RH controls across a wide range of temperatures is shown in Table S4. The illumination of lamps raises the lowest achievable temperature by 3 ℃ for every 10 lights on. However, the illumination of the reactor does not affect the stability of temperature and RH inside the reactor. When the set temperature is close to room temperature (20 ℃ in Table S4), the fluctuation is < 0.1 ℃, demonstrating a more accurate temperature and RH control performance compared with other chambers (Table S5) (Wang et al., 2014; Wu et al., 2007; Bin Babar et al., 2016; Ma et al., 2022; Wang et al., 2015b). Sampling operation (lasting more than 3 hours with flow rate at 5 L/min, Fig. 2) does not significantly affect the stability of temperature and RH control either, which also indicates the permeation and wall loss of water molecules do not affect a lot.

In order to simulate the diurnal variations in ambient air temperature and RH, a proportional-integral-derivative (PID) feedback controlling function was designed. The RH in the reactor can reach the target RH by controlling the temperature. After receiving the target RH input, the control program calculates the stepwise theoretical RH value at each time increment and the corresponding temperature control steps based on current temperature and RH in the reactor. This calculation is also adjusted in real-time to optimize the gradual change of RH. Figure S7 demonstrates two examples to show alternate linear change and constant control of RH. The RH can reach the set value within a few hours with fluctuations < 0.75%. This function performs even better at low temperatures, suggesting the potential of using this chamber system to simulate diurnal variations of RH in the ambient atmosphere in wintertime.

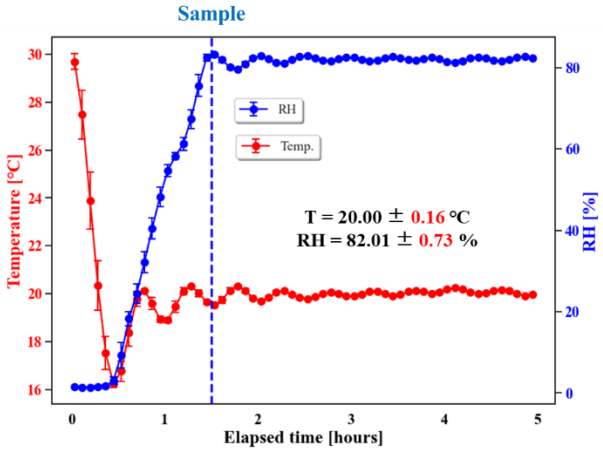

Figure 2. Stability of temperature and RH control in the reactor during sampling. The chamber was operated in batch mode.

3.4 Wall loss of gas and particles

The wall loss process is considered as a first-order kinetic process, in that the decay rate of a concentration is proportional to the concentration:

$$\frac{dC(t)}{dt} = -k \cdot C(t) \quad (1)$$

where C(t) is the species concentration at time t, and k is the wall loss rate constant (in units: s^{-1} or min^{-1}). The wall loss rates of gaseous species such as NO_x and O_3 in this study are shown in Table S6, the values of which are lower than other small Teflon chambers (2 ~ 5 m^3) (Wu et al., 2007; Wang et al., 2015b; Li et al., 2017; Bernard et al., 2016), as a result of passivation of the inner surface of the reactor with 2 ppm O_3 for 3 days. In Table S6, when turn on the fans, the wall loss is usually much higher, so the fans will only be turned on during the injection period, and when simulating the reaction and sampling, the fans are kept off.

The wall loss rate constant k of particles is dependent on particle size (diameter, noted as D_p). Smaller or larger particles often have higher k values (Crump and Seinfeld, 1981) due to higher diffusion or sedimentation rates, respectively. The dependence of k values for particles with D_p < 50 nm is rarely reported in previous chamber studies. This study demonstrates that the constant k decreases as a function of decreasing D_p when particles are smaller than 50 nm, which is also shown in Fig. S7 of Ma et al (Ma et al., 2022). The $\log_{10}(k)$ value for particles can be approximated with a segmented linear function of $\log_{10}(D_p)$ [93, 94]. In addition to the slopes to be determined, the inflection point D_p, where the loss trend inverses, changes with different chambers. In this study, two inflection points are selected at 50 nm and 150 nm according to the identified inflection particle size bin of 45.3 – 53.2 nm and 143.3 – 165.5 nm, respectively (Fig. S8). Furthermore, the k-Dp dependence has been reported to deviate in different experiments even in the same reactor. This study found that such deviations can be corrected through an up-and-down shift of the $\log_{10}(k)$-$\log_{10}(Dp)$ function curve. Even for deliquescent particles (RH = 90 % in Fig. S8, the Dp of the x-axis represents the liquid particle diameters), this method still accurately described the relationship between k and Dp (R^2~0.95) when considering the hygroscopic growth of the particle size.

Another commonly used parameter to characterize the particle wall loss behavior in chambers is the total volume wall loss rate constant (k_v). For small Teflon chambers of 2 ~ 3 m^3 in size (Takekawa et al., 2003; Li et al., 2017; Liu et al., 2019), k_v values typically range from 2.84 ~ 4.72 × 10^{-3} min^{-1}. The particle wall

loss is slightly higher in the chamber in this study, with the k_v found to be 5×10^{-3} min^{-1} (Table S7).

3.5 Morphology of seed particle generation

Seed particles are typically used to simulate aerosol formation by the multiphase chemistry pathway. The AIR chamber is designed to couple to a subsystem for generating seed particles with different phase states through pre-deliquescing, adopted from a previous study (Faust et al., 2017). A volatilizing-condensing method is used to generate known-composition organic-coated inorganic particles in the AIR chamber, with a detailed description in Section 2.4.

As shown in Figure 3, squalane is coated onto dry 200-nm monodisperse NaCl seed particles to produce a core-shell morphology for the particles. The coating thickness is controlled by adjusting the water bath heating temperature while maintaining a fixed condensation temperature of 20 °C. The surface area concentrations of the introduced seed (> 800 $\mu m^2/cm^3$) are sufficient that no homogeneous nucleation of organic vapor occurs. Both the size distributions of the particles before and after condensing organics on the particles are monodisperse. Using the Clausius-Clapeyron equation that describes the relationship between saturation vapor pressure and temperature, as well as the Maxwell equation that describes the condensation growth rate of particle size under a certain supersaturated vapor pressure, the coating thickness can be predicted in relation to the heating temperature (Fig. 3a), to assess the feasibility of the selected coating species. The coating thickness is calculated as half of the difference in peak Dp of the monodisperse particle size distribution before and after the seeds are coated (Fig. 3b). For squalane, the device allows for a relatively accurate control of coating thickness in the range of 5 to 25 nm (1 % ~ 12 % shell thickness). For organic species with similar volatilities (saturated vapor pressure in the order of 10^{-4} ~ 10^{-5} mmHg at room temperature), the device could provide similar control performance.

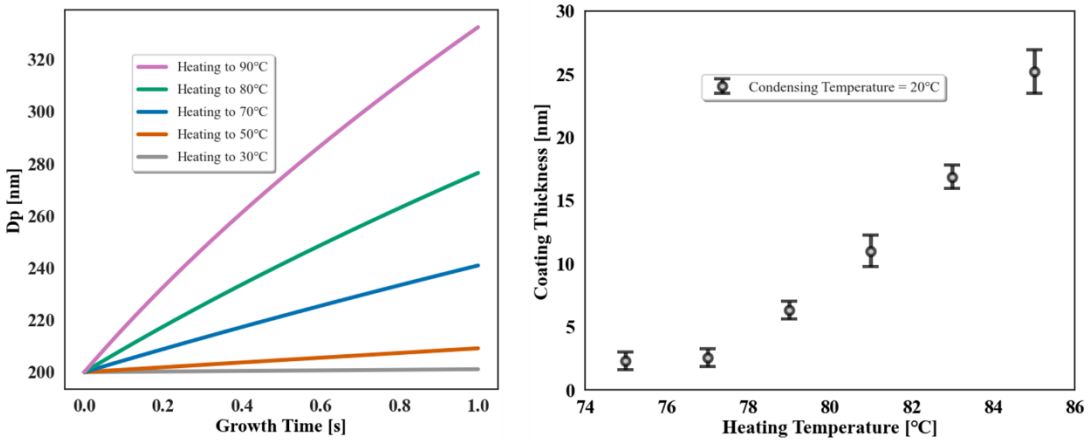

Figure 3. Relationship between coating thickness on dry 200 nm NaCl seed and heating temperature in the coating device, with squalane as the coating species and 20 ℃ condensing temperature. (a) Theoretical estimation in different growth times. (b) Measured results by SMPS.

4 Applications in SOA generation——α-pinene ozonolysis researches

4.1 SOA yield of seed-absent experiments

SOA are generated from α-pinene ozonolysis in the AIR chamber to evaluate its performance, with experiment conditions given in Table S8 (NO.1 ~ 5). The key parameter Y, representing the yield of SOA, is defined as:

$$Y = \frac{\Delta mo}{\Delta ROG} \quad (2)$$

where Δmo represents the total mass concentration of generated SOA, and ΔROG represents the total mass concentration of reactive organic gas that was consumed in the reaction (specifically referring to α-pinene in this study), with both units in μg/m^3. SOA mass concentration was measured by a ToF-ACSM (Section 2.5). The organic mass measurement was also corrected based on the particle size distribution data from SMPS, where the α-pinene-derived SOA density was assumed as 1.3 g/cm^3. This density value is also used in many previous researches (Bahreini et al., 2005; Alfarra et al., 2006; Ma et al., 2022), but higher than the unit density assumption used in some other chamber studies (Wang et al., 2011; Wang et al., 2014; Bin Babar et al., 2016; Cocker Iii et al., 2001; Li et al., 2021; Zhang et al., 2015).

Odum et al (Odum et al., 1996) found that the two-product model reproduces well the non-linear relationship between the SOA yield Y and the particulate organic mass concentration (mo):

$$Y = mo \cdot \sum \frac{\alpha_i \cdot K_{om,i}}{1+mo \cdot K_{om,i}} \quad (3)$$

where α_i and $K_{om,i}$ are the mass-based stoichiometric and partition coefficient for species i, respectively, and mo is the total mass concentration of organic aerosol. Figure 4 shows the results of the two-product model that fits the seed-absent SOA yield results in this study. The Odum model fits results from other chamber studies are also shown in Figure 4 for comparison. Detailed model fitting parameters are shown in Table S9. In contrast, Y in this study is a little higher than those in other small or medium-sized chambers, which may be owing to the lower gas wall loss in our Teflon reactor (Section 3.4) and the lower experimental temperature. The four fitting parameters in this study, α1, α2, K1, K2, are 0.62479, 0.0326791, 0.0121589, 0.0121596, respectively. K1 and K2 are close and are moderate values; however,

α1 is significantly higher than those in other chambers. Such higher value for α1 can be an indication of a lower volatilizing loss of the gas phase intermediates within the AIR reactor compared with the other chambers. The good fitting from our experiment indicates that the chamber system in this study is stable. These results imply a reliable performance of our chamber system for experimental simulation studies of atmospheric secondary transformation process.

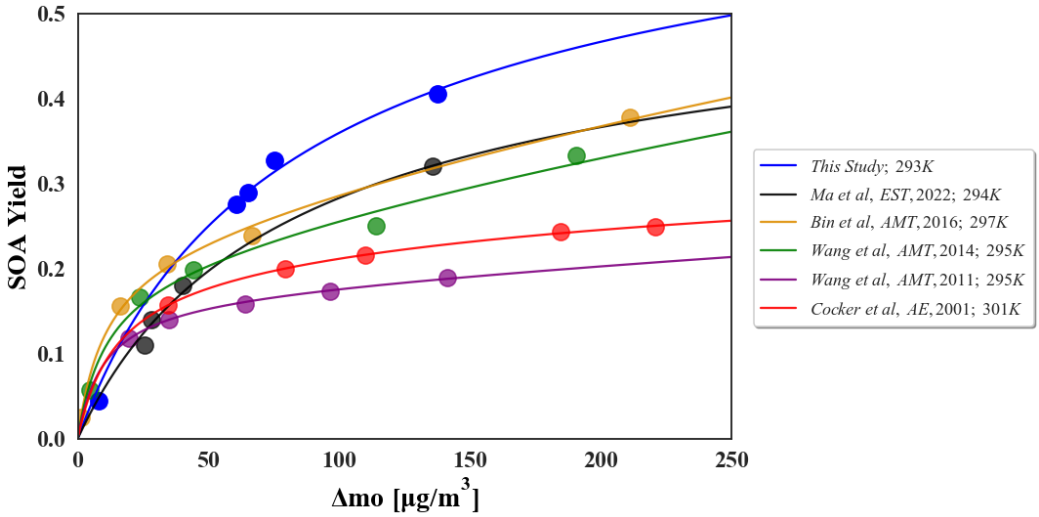

Figure 4. Two-product model fitting curve of seed-absent α-pinene-derived SOA yield in this study and the comparison with other literature results. The data of the blue line is from this study, and other data is obtained from these references (Cocker Iii et al., 2001; Wang et al., 2011; Wang et al., 2014; Bin Babar et al., 2016; Ma et al., 2022).

4.2 Effects of seed phase state on SOA yield

The effects of different seed phase state on the yield of α-pinene-derived SOA were further investigated using ammonium sulfate as the seed particles (Table S8, NO.6 ~ 8). We used seeds with sufficient surface area concentration to prevent the gas phase products of VOC from homogeneous nucleation. Figure S11 shows the relevant measured parameters during one reaction (e.g., experiment NO.8). The yields of all the experiments are summarized in Fig. 5. In general, the yield in the presence of dry seeds is not significantly different from that in the absence of seeds, consistent with the outcome of Odum et al (Odum et al., 1996). However, in the presence of aerosol liquid water and ammonium sulfate seeds, the α-pinene-derived SOA yield is reduced. This suppressing phenomenon is also reported by Cocker et al (Cocker Iii et al., 2001), which may be related to the finding of Lutz et al (Lutz et al., 2019) that an inhibition of organic species partitioning in the particulate phase exists at high sulfates level. However, to our knowledge, the suppressing phenomenon above may not be common, that has only been reported in the

α-pinene ozonolysis system with ammonium sulfate seeds.

The subplot in Fig. 5 demonstrates the SOA yield at each elapsed time point in these experiments. Liquid water can significantly promote the initial SOA yield and generation rate (Zhang et al., 2018), and our results have reproduced this phenomenon (subplot in Fig. 5). However, the oxidation reaction proceeds, it is observed that the SOA yield with liquid seeds decreases, and larger seed aerosol liquid water contents produce greater decreases in the yield. These indicate the AIR chamber system facilitates the researches of aerosol properties on atmospheric multiphase processes.

It is worth noting that, the organic vapor wall loss can have significant influence on SOA formation. However, quantifying wall losses of gaseous organic products is still a challenge in chamber experiments. Gaseous intermediates are difficult to be quantitatively measured, and the theoretical calculations of wall losses also have large uncertainties due to the lack of data on some parameters, such as the effective wall mass concentration and eddy diffusion coefficient inside the reactor. The wall loss behavior of gases essentially depends on the concentration gradient between the gas phase and the wall. To our knowledge, there is no conclusive evidence to support higher wall losses of gaseous intermediates under higher RH, which are even significant enough to cause a notable reduction in SOA yield. In addition, if higher RH can enhance the diffusion of gaseous intermediates towards the wall, then the diffusion of gaseous intermediates towards the particle phase should also increase. Compared with experiments without seed particles, when seed particles exist, gases condense on the particles while condensing on the walls, causing the gas-phase concentration to decay more rapidly, resulting in less wall loss of gases and higher SOA yields during the initial period of the experiment, as shown in the subplot of Fig. 5. However, the final difference in SOA yields is still unclear because, under the condition without seed particles, particles generated through nucleation continue to grow and can provide a considerable amount of condensation sink after the reaction proceeds for a period of time. This process needs to be numerically described and analyzed that carefully consider wall loss behavior and physicochemical properties of particles in future studies.

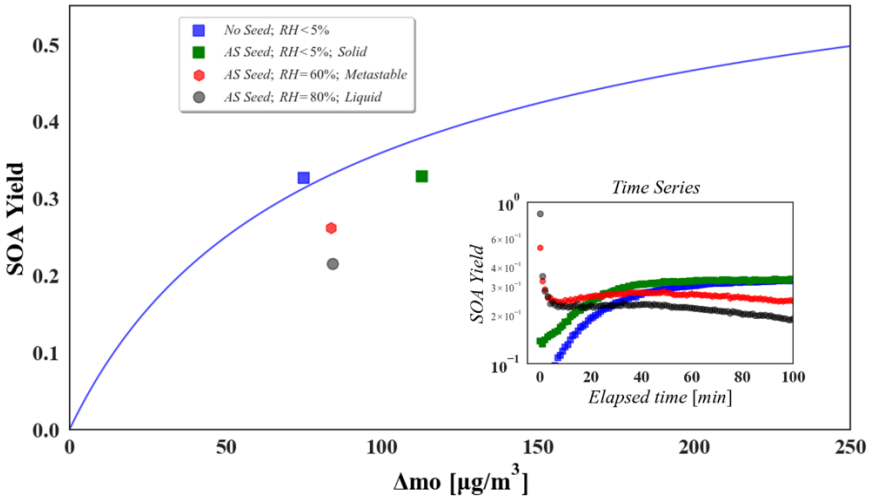

Figure 5. Effects of phase state and liquid water content of ammonium sulfate seed particles on the SOA yield of α-pinene ozonolysis (α-pinene = 60 ±13 ppb, O3 = 296 ±30 ppb). In the main plot, the blue line is the fitting two-product curve from no-seed experiments data in this study, which is a replicate of the curve in Fig. 4. The subplot shows the current yield since the initial time point of each experiment, where the blue points represent the data of no-seed experiment, green points represent the data of solid seed experiment, red points represent the data of metastable seed experiment, and grey points represent the data of liquid seed experiment.

5 Conclusions

The reported special phenomena relying on specific particle properties are well reproduced in AIR chamber benefitting from the seed phase state control, and the accurate temperature and RH control facilitates the quantization of the effects of aerosol liquid water. Besides, compared to other chambers, the manipulation of composition and thickness of organic coating could provide a more clarity surface property. Broad temperature range, adjustable irradiation intensity, and the fast-responding RH cycle, make this chamber system suitable for simulating diurnal ambient atmosphere in different seasons. These performances of handling key parameters suggest the potential of this AIR chamber system for the laboratory simulation of atmospheric multiphase processes.

Data availability

The data in this study are available from the authors upon request (zhijunwu@pku.edu.cn).

Acknowledgements

We thank the Beijing Convenient Environmental Tech Co. Ltd. for constructing the chamber.

Financial support

This research was financially supported by the National Natural Science Foundation of China (41875149).

Author contributions

TZ and ZW conceived the study. TZ, ZW, JW, WF conducted the laboratory measurements. TZ carried out the data analysis. TZ, KB, YY, XY, ZB, XM, YZ participated in the instrument managements. SG, YC, CL, YZ, S-ML and MH supported this research. TZ wrote the paper with inputs from all co-authors.

Competing interest

The authors declare that they have no known competing financial interests or personal relationships that could have appeared to influence the work reported in this paper.

References

Abbatt, J. P., Lee, A. K., and Thornton, J. A.: Quantifying trace gas uptake to tropospheric aerosol: recent advances and remaining challenges, Chemical Society reviews, 41, 6555-6581, 10.1039/c2cs35052a, 2012.

Akimoto, H., Hoshino, M., Inoue, G., Sakamaki, F., Washida, N., and Okuda, M.: Design and characterization of the evacuable and bakable photochemical smog chamber, Environ.sci.technol, 13, 471-475, 1979.

Albu, M., Barnes, I., and Mocanu, R.: Kinetic Study of the Temperature Dependence of the OH Initiated Oxidation of Dimethyl Sulphide, Dordrecht, 223-230, 2006.

Alfarra, M. R., Paulsen, D., Gysel, M., Garforth, A. A., Dommen, J., Prevot, A. S. H., Worsnop, D. R., Baltensperger, U., and Coe, H.: A mass spectrometric study of secondary organic aerosols formed from the photooxidation of anthropogenic and biogenic precursors in a reaction chamber, Atmospheric Chemistry And Physics, 6, 5279-5293, 2006.

Atkinson, R., Baulch, D. L., Cox, R. A., Crowley, J. N., Hampson, R. F., Hynes, R. G., Jenkin, M. E., Rossi, M. J., and Troe, J.: Evaluated kinetic and photochemical data for atmospheric chemistry: Volume I - gas phase reactions of O-x, HOx, NOx and SOx species, Atmospheric Chemistry And Physics, 4, 1461-1738, 2004.

Bahreini, R., Keywood, M. D., Ng, N. L., Varutbangkul, V., Gao, S., Flagan, R. C., Seinfeld, J. H., Worsnop, D. R., and Jimenez, J. L.: Measurements of secondary organic aerosol from oxidation of cycloalkenes, terpenes, and m-xylene using an Aerodyne aerosol mass spectrometer, Environmental Science & Technology, 39, 5674-5688, 2005.

Barnes, I.: Kinetics, Products and Mechanism of O(3P) Atom Reactions with Alkyl Iodides, Environmental Simulation Chambers: Application to Atmospheric Chemical Processes, Dordrecht, 193-

205, 2006.
Batchvarova, E., Spassova, T., Valkov, N., and Iordanova, L.: Survey on Atmospheric Chemistry Research in Some New EU Member States and Candidate Countries, Dordrecht, 301-340, 2006.
Bejan, I., Barnes, I., Olariu, R., Becker, K. H., and Mocanu, R.: FT-IR Kinetic Study on the Gas-Phase Reactions of the OH Radical with a Series of Nitroaromatic Compounds, Dordrecht, 155-162, 2006.
Berkemeier, T., Steimer, S. S., Krieger, U. K., Peter, T., Poschl, U., Ammann, M., and Shiraiwa, M.: Ozone uptake on glassy, semi-solid and liquid organic matter and the role of reactive oxygen intermediates in atmospheric aerosol chemistry, Physical chemistry chemical physics : PCCP, 18, 12662-12674, 10.1039/c6cp00634e, 2016.
Bernard, F., Ciuraru, R., Boreave, A., and George, C.: Photosensitized Formation of Secondary Organic Aerosols above the Air/Water Interface, Environmental Science & Technology, 50, 8678-8686, 2016.
Bin Babar, Z., Park, J. H., Kang, J., and Lim, H. J.: Characterization of a Smog Chamber for Studying Formation and Physicochemical Properties of Secondary Organic Aerosol, Aerosol Air Qual Res, 16, 3102-3113, 2016.
Bohn, B., Rohrer, F., Brauers, T., and Wahner, A.: Actinometric measurements of NO2 photolysis frequencies in the atmosphere simulation chamber SAPHIR, ATMOSPHERIC CHEMISTRY AND PHYSICS, 5, 493-503, 2004.
Brauers, T., Bohn, B., Johnen, F.-J., Rohrer, R., Rodriguez Bares, S., Tillmann, R., and Wahner, A.: The atmosphere simulation chamber SAPHIR: a tool for the investigation of photochemistry, Nice, 4449, 2003.
Brunamonti, S., Krieger, U. K., Marcolli, C., and Peter, T.: Redistribution of black carbon in aerosol particles undergoing liquid-liquid phase separation, Geophysical Research Letters, 42, 2532-2539, 2015.
Carter, W. P. L.: Environmental Chamber Studies of Ozone Formation Potentials of Volatile Organic Compounds, Dordrecht, 231-240, 2006.
Carter, W. P. L. and Lurmann, F. W.: Evaluation Of a Detailed Gas-Phase Atmospheric Reaction-Mechanism Using Environmental Chamber Data, Atmos Environ a-Gen, 25, 2771-2806, 1991.
Carter, W. P. L., Atkinson, R., Winer, A. M., and Pitts, J. N.: Experimental Investigation Of Chamber-Dependent Radical Sources, International Journal Of Chemical Kinetics, 14, 1071-1103, 1982.
Carter, W. P. L., Cocker, D. R., Fitz, D. R., Malkina, I. L., Bumiller, K., Sauer, C. G., Pisano, J. T., Bufalino, C., and Song, C.: A new environmental chamber for evaluation of gas-phase chemical mechanisms and secondary aerosol formation, Atmospheric Environment, 39, 7768-7788, 2005.
Chen, B. B. and Lelevkin, V. M.: Influence of Atmospheric Aerosol Contamination on the Regional Climate in Central Asia, Dordrecht, 403-414, 2006.
Chen, T. Z., Liu, Y. C., Liu, C. G., Liu, J., Chu, B. W., and He, H.: Important role of aromatic hydrocarbons in SOA formation from unburned gasoline vapor, Atmospheric Environment, 201, 101-109, 2019a.
Chen, T. Z., Liu, Y. C., Ma, Q. X., Chu, B. W., Zhang, P., Liu, C. G., Liu, J., and He, H.: Significant source of secondary aerosol: formation from gasoline evaporative emissions in the presence of SO_2 and NH3, Atmospheric Chemistry And Physics, 19, 8063-8081, 2019b.
Cheng, Y., Su, H., Koop, T., Mikhailov, E., and Poschl, U.: Size dependence of phase transitions in aerosol nanoparticles, Nature communications, 6, 5923, 10.1038/ncomms6923, 2015.
Cocker, D. R., Flagan, R. C., and Seinfeld, J. H.: State-of-the-art chamber facility for studying atmospheric aerosol chemistry, Environmental Science & Technology, 35, 2594-2601, 2001.
Cocker Iii, D. R., Clegg, S. L., Flagan, R. C., and Seinfeld, J. H.: The effect of water on gas–particle

599 partitioning of secondary organic aerosol. Part I: α-pinene/ozone system, Atmospheric Environment, 35,
600 6049-6072, https://doi.org/10.1016/S1352-2310(01)00404-6, 2001.
601 Corral Arroyo, P., Bartels-Rausch, T., Alpert, P. A., Dumas, S., Perrier, S., George, C., and Ammann, M.:
602 Particle-Phase Photosensitized Radical Production and Aerosol Aging, Environ Sci Technol, 52, 7680-
603 7688, 10.1021/acs.est.8b00329, 2018.
604 Cosman, L. M. and Bertram, A.: Reactive Uptake of N 2 O 5 on Aqueous H 2 SO 4 Solutions Coated
605 with 1-Component and 2-Component Monolayers, Journal of Physical Chemistry A, 112, 4625, 2008.
606 Crump, J. G. and Seinfeld, J. H.: Turbulent Deposition And Gravitational Sedimentation Of an Aerosol
607 In a Vessel Of Arbitrary Shape, Journal Of Aerosol Science, 12, 405-415, 1981.
608 Davidovits, P., Kolb, C. E., Williams, L. R., Jayne, J. T., and Worsnop, D. R.: Update 1 of: Mass
609 Accommodation and Chemical Reactions at Gas−Liquid Interfaces, Chemical reviews, 111,
610 10.1021/cr100360b, 2011.
611 Dodge, M. C.: Chemical oxidant mechanisms for air quality modeling: critical review, Atmospheric
612 Environment, 34, 2103-2130, 2000.
613 Faust, J. A., Wong, J. P., Lee, A. K., and Abbatt, J. P.: Role of Aerosol Liquid Water in Secondary Organic
614 Aerosol Formation from Volatile Organic Compounds, Environ Sci Technol, 51, 1405-1413,
615 10.1021/acs.est.6b04700, 2017.
616 Fleming, L. T., Lin, P., Roberts, J. M., Selimovic, V., Yokelson, R., Laskin, J., Laskin, A., and Nizkorodov,
617 S. A.: Molecular composition and photochemical lifetimes of brown carbon chromophores in biomass
618 burning organic aerosol, Atmospheric Chemistry And Physics, 20, 1105-1129, 2020.
619 Franco, B., Blumenstock, T., Cho, C., Clarisse, L., Clerbaux, C., Coheur, P. F., De Maziere, M., De Smedt,
620 I., Dorn, H. P., Emmerichs, T., Fuchs, H., Gkatzelis, G., Griffith, D. W. T., Gromov, S., Hannigan, J. W.,
621 Hase, F., Hohaus, T., Jones, N., Kerkweg, A., Kiendler-Scharr, A., Lutsch, E., Mahieu, E., Novelli, A.,
622 Ortega, I., Paton-Walsh, C., Pommier, M., Pozzer, A., Reimer, D., Rosanka, S., Sander, R., Schneider,
623 M., Strong, K., Tillmann, R., Van Roozendael, M., Vereecken, L., Vigouroux, C., Wahner, A., and
624 Taraborrelli, D.: Ubiquitous atmospheric production of organic acids mediated by cloud droplets, Nature,
625 593, 233-237, 10.1038/s41586-021-03462-x, 2021.
626 George, C., Ammann, M., D'Anna, B., Donaldson, D. J., and Nizkorodov, S. A.: Heterogeneous
627 photochemistry in the atmosphere, Chemical reviews, 115, 4218-4258, 10.1021/cr500648z, 2015.
628 George, I. J. and Abbatt, J. P.: Heterogeneous oxidation of atmospheric aerosol particles by gas-phase
629 radicals, Nature chemistry, 2, 713-722, 10.1038/nchem.806, 2010.
630 Griffin, R. J., Cocker, D. R., Flagan, R. C., and Seinfeld, J. H.: Organic aerosol formation from the
631 oxidation of biogenic hydrocarbons, Journal Of Geophysical Research-Atmospheres, 104, 3555-3567,
632 1999.
633 Haagensmit, A. J.: Chemistry And Physiology Of Los-Angeles Smog, Industrial And Engineering
634 Chemistry, 44, 1342-1346, 1952.
635 Hallquist, M., Wenger, J. C., Baltensperger, U., Rudich, Y., Simpson, D., Claeys, M., Dommen, J.,
636 Donahue, N. M., George, C., Goldstein, A. H., Hamilton, J. F., Herrmann, H., Hoffmann, T., Iinuma, Y.,
637 Jang, M., Jenkin, M. E., Jimenez, J. L., Kiendler-Scharr, A., Maenhaut, W., McFiggans, G., Mentel, T.
638 F., Monod, A., Prevot, A. S. H., Seinfeld, J. H., Surratt, J. D., Szmigielski, R., and Wildt, J.: The formation,
639 properties and impact of secondary organic aerosol: current and emerging issues, Atmospheric Chemistry
640 And Physics, 9, 5155-5236, 2009.
641 Herrmann, H., Schaefer, T., Tilgner, A., Styler, S. A., Weller, C., Teich, M., and Otto, T.: Tropospheric
642 aqueous-phase chemistry: kinetics, mechanisms, and its coupling to a changing gas phase, Chemical

reviews, 115, 4259-4334, 10.1021/cr500447k, 2015.
Hidy, G. M.: Atmospheric Chemistry in a Box or a Bag, Atmosphere-Basel, 10, 401, 2019.
Hu, C. J., Cheng, Y., Pan, G., Gai, Y. B., Gu, X. J., Zhao, W. X., Wang, Z. Y., Zhang, W. J., Chen, J., Liu, F. Y., Shan, X. B., and Sheng, L. S.: A Smog Chamber Facility for Qualitative and Quantitative Study on Atmospheric Chemistry and Secondary Organic Aerosol, Chinese J Chem Phys, 27, 631-639, 2014.
Hurley, M. D., Sokolov, O., Wallington, T. J., Takekawa, H., Karasawa, M., Klotz, B., Barnes, I., and Becker, K. H.: Organic aerosol formation during the atmospheric degradation of toluene, Environmental Science & Technology, 35, 1358-1366, 2001.
Johnson, D., Jenkin, M. E., Wirtz, K., and Martin-Reviejo, M.: Simulating the Formation of Secondary Organic Aerosol from the Photooxidation of Toluene, Environmental Chemistry, 1, 150-165, 2004.
Kang, E., Root, M. J., Toohey, D. W., and Brune, W. H.: Introducing the concept of Potential Aerosol Mass (PAM), Atmospheric Chemistry And Physics, 7, 5727-5744, 2007.
Kolev, S. and Grigorieva, V.: Surface and Total Ozone Over Bulgaria, Dordrecht, 351-358, 2006.
Lambe, A. T., Chhabra, P. S., Onasch, T. B., Brune, W. H., Hunter, J. F., Kroll, J. H., Cummings, M. J., Brogan, J. F., Parmar, Y., Worsnop, D. R., Kolb, C. E., and Davidovits, P.: Effect of oxidant concentration, exposure time, and seed particles on secondary organic aerosol chemical composition and yield, Atmospheric Chemistry and Physics, 15, 3063-3075, 10.5194/acp-15-3063-2015, 2015.
Lane, D. A. and Tang, H.: Photochemical Degradation of Polycyclic Aromatic Compounds. I. Naphthalene, Polycyclic Aromatic Compounds, 5, 131-138, 1994.
Leone, J. A., Flagan, R. C., Grosjean, D., and Seinfeld, J. H.: An Outdoor Smog Chamber And Modeling Study Of Toluene-Nox Photooxidation, International Journal Of Chemical Kinetics, 17, 177-216, 1985.
Leone, J. A., Flagan, R. C., Grosjean, D., and Seinfeld, J. H.: An outdoor smog chamber and modeling study of toluene–NOx photooxidation, International Journal of Chemical Kinetics, 17, 177-216, 2010.
Li, J. L., Li, H., Wang, X. Z., Wang, W. G., Ge, M. F., Zhang, H., Zhang, X., Li, K., Chen, Y., Wu, Z. H., Chai, F. H., Meng, F., Mu, Y. J., Mellouki, A., Bi, F., Zhang, Y. J., Wu, L. Y., and Liu, Y. C.: A large-scale outdoor atmospheric simulation smog chamber for studying atmospheric photochemical processes: Characterization and preliminary application, J Environ Sci-China, 102, 185-197, 2021.
Li, K. W., Chen, L. H., Han, K., Lv, B. A., Bao, K. J., Wu, X. C., Gao, X., and Cen, K. F.: Smog chamber study on aging of combustion soot in isoprene/SO2/NOx system: Changes of mass, size, effective density, morphology and mixing state, Atmospheric Research, 184, 139-148, 2017.
Liu, S. J., Tsona, N. T., Zhang, Q., Jia, L., Xu, Y. F., and Du, L.: Influence of relative humidity on cyclohexene SOA formation from OH photooxidation, Chemosphere, 231, 478-486, 2019.
Liu, T., Chan, A. W. H., and Abbatt, J. P. D.: Multiphase Oxidation of Sulfur Dioxide in Aerosol Particles: Implications for Sulfate Formation in Polluted Environments, Environ Sci Technol, 55, 4227-4242, 10.1021/acs.est.0c06496, 2021.
Liu, T. Y. and Abbatt, J. P. D.: Oxidation of sulfur dioxide by nitrogen dioxide accelerated at the interface of deliquesced aerosol particles, Nature chemistry, 13, 1173-1177, 10.1038/s41557-021-00777-0, 2021.
Lutz, A., Mohr, C., Le Breton, M., Lopez-Hilfiker, F. D., Priestley, M., Thornton, J. A., and Hallquist, M.: Gas to Particle Partitioning of Organic Acids in the Boreal Atmosphere, ACS Earth and Space Chemistry, 3, 1279-1287, 10.1021/acsearthspacechem.9b00041, 2019.
Ma, W., Liu, Y., Zhang, Y., Feng, Z., Zhan, J., Hua, C., Ma, L., Guo, Y., Zhang, Y., Zhou, W., Yan, C., Chu, B., Chen, T., Ma, Q., Liu, C., Kulmala, M., Mu, Y., and He, H.: A New Type of Quartz Smog Chamber: Design and Characterization, Environ Sci Technol, 56, 2181-2190, 10.1021/acs.est.1c06341, 2022.

Martin-Reviejo, M. and Wirtz, K.: Is benzene a precursor for secondary organic aerosol?, Environmental Science & Technology, 39, 1045-1054, 2005.
Mekic, M., Liu, J., Zhou, W., Loisel, G., and Gligorovski, S.: Formation of highly oxygenated multifunctional compounds from cross-reactions of carbonyl compounds in the atmospheric aqueous phase, Atmospheric Environment, 219, 117046, 2019.
Mellouki, A.: Atmospheric Fate of Unsaturated Ethers, Dordrecht, 163-169, 2006.
Mocanu, R., Cucu-Man, S., and Steinnes, E.: Heavy Metals Pollution: An Everlasting Problem, Dordrecht, 359-368, 2006.
Morriss, F. V., Bolze, C., Goodwin, J. T., and King, F.: Smog Experiments In Large Chambers, Industrial And Engineering Chemistry, 49, 1249-1250, 1957.
Odum, J. R., Hoffmann, T., Bowman, F., Collins, D., Flagan, R. C., and Seinfeld, J. H.: Gas/particle partitioning and secondary organic aerosol yields, Environmental Science & Technology, 30, 2580-2585, 1996.
Odum, J. R., Jungkamp, T. P. W., Griffin, R. J., Forstner, H. J. L., Flagan, R. C., and Seinfeld, J. H.: Aromatics, reformulated gasoline, and atmospheric organic aerosol formation, Environmental Science & Technology, 31, 1890-1897, 1997.
Olariu, R.-I., Duncianu, M., Arsene, C., and Wirtz, K.: Determination of Photolysis Frequencies for Selected Carbonyl Compounds in the EUPHORE Chamber Environmental, Dordrecht, 121-128, 2006.
Pöschl, U. and Shiraiwa, M.: Multiphase chemistry at the atmosphere-biosphere interface influencing climate and public health in the anthropocene, Chemical reviews, 115, 4440-4475, 10.1021/cr500487s, 2015.
Pandis, S. N., Paulson, S. E., Seinfeld, J. H., and Flagan, R. C.: Aerosol Formation In the Photooxidation Of Isoprene And Beta-Pinene, Atmos Environ a-Gen, 25, 997-1008, 1991.
Paulsen, Dommen, Kalberer, Prevot, ASH, Richter, Sax, Steinbacher, Weingartner, and Baltensperger: Secondary organic aerosol formation by irradiation of 1,3,5-trimethylbenzene-NOx-H2O in a new reaction chamber for atmospheric chemistry and physics, Environmental Science & Technology, 39, 2668-2678, https://doi.org/10.1021/es0489137, 2005.
Peng, J., Hu, M., Guo, S., Du, Z., Shang, D., Zheng, J., Zheng, J., Zeng, L., Shao, M., Wu, Y., Collins, D., and Zhang, R.: Ageing and hygroscopicity variation of black carbon particles in Beijing measured by a quasi-atmospheric aerosol evolution study (QUALITY) chamber, Atmospheric Chemistry and Physics, 17, 10333-10348, 10.5194/acp-17-10333-2017, 2017.
Platt, S. M., El Haddad, I., Zardini, A. A., Clairotte, M., Astorga, C., Wolf, R., Slowik, J. G., Temime-Roussel, B., Marchand, N., Jezek, I., Drinovec, L., Mocnik, G., Mohler, O., Richter, R., Barmet, P., Bianchi, F., Baltensperger, U., and Prevot, A. S. H.: Secondary organic aerosol formation from gasoline vehicle emissions in a new mobile environmental reaction chamber, Atmospheric Chemistry And Physics, 13, 9141-9158, 2013.
Pratap, V., Carlton, A. G., Christiansen, A. E., and Hennigan, C. J.: Partitioning of Ambient Organic Gases to Inorganic Salt Solutions: Influence of Salt Identity, Ionic Strength, and pH, Geophysical Research Letters, 48, 10.1029/2021gl095247, 2021.
Ravishankara, A. R.: Heterogeneous and multiphase chemistry in the troposphere, Science, 276, 1058-1065, 1997.
Reid, J. P., Bertram, A. K., Topping, D. O., Laskin, A., Martin, S. T., Petters, M. D., Pope, F. D., and Rovelli, G.: The viscosity of atmospherically relevant organic particles, Nature communications, 9, 956, 10.1038/s41467-018-03027-z, 2018.

Ren, Y. G., Grosselin, B., Daele, V., and Mellouki, A.: Investigation of the reaction of ozone with isoprene, methacrolein and methyl vinyl ketone using the HELIOS chamber, Faraday Discussions, 200, 289-311, 2017.
Rollins, A. W., Kiendler-Scharr, A., Fry, J. L., Brauers, T., Brown, S. S., Dorn, H. P., Dube, W. P., Fuchs, H., Mensah, A., Mentel, T. F., Rohrer, F., Tillmann, R., Wegener, R., Wooldridge, P. J., and Cohen, R. C.: Isoprene oxidation by nitrate radical: alkyl nitrate and secondary organic aerosol yields, Atmospheric Chemistry And Physics, 9, 6685-6703, 2009.
Rudzinski, K. J.: Heterogeneous and Aqueous-Phase Transformations of Isoprene, Dordrecht, 261-277,
Stern, J. E., Flagan, R. C., Grosjean, D., and Seinfeld, J. H.: Aerosol Formation And Growth In Atmospheric Aromatic Hydrocarbon Photooxidation, Environmental Science & Technology, 21, 1224-1231, 1987.
Su, H., Cheng, Y., and Poschl, U.: New Multiphase Chemical Processes Influencing Atmospheric Aerosols, Air Quality, and Climate in the Anthropocene, Accounts of chemical research, 53, 2034-2043, 10.1021/acs.accounts.0c00246, 2020.
Su, H., Cheng, Y., Zheng, G., Wei, C., Mu, Q., Zheng, B., Wang, Z., Zhang, Q., He, K., and Carmichael, G.: Reactive nitrogen chemistry in aerosol water as a source of sulfate during haze events in China, Science Advances, 2, e1601530-e1601530, 2016.
Takekawa, H., Minoura, H., and Yamazaki, S.: Temperature dependence of secondary organic aerosol formation by photo-oxidation of hydrocarbons, Atmospheric Environment, 37, 3413-3424, 2003.
Thuner, L. P., Bardini, P., Rea, G. J., and Wenger, J. C.: Kinetics of the gas-phase reactions of OH and NO3 radicals with dimethylphenols, Journal Of Physical Chemistry A, 108, 11019-11025, 2004.
Tolkacheva, G. A.: Problems of Air Quality in Tashkent City, Dordrecht, 379-392, 2006.
Turšič, J., Grgić, I., and Podkrajšek, B.: Influence of ionic strength on aqueous oxidation of SO2 catalyzed by manganese, Atmospheric Environment, 37, 2589-2595, 10.1016/s1352-2310(03)00215-2, 2003.
Virtanen, A., Joutsensaari, J., Koop, T., Kannosto, J., Yli-Pirila, P., Leskinen, J., Makela, J. M., Holopainen, J. K., Poschl, U., Kulmala, M., Worsnop, D. R., and Laaksonen, A.: An amorphous solid state of biogenic secondary organic aerosol particles, Nature, 467, 824-827, 10.1038/nature09455, 2010.
Wang, B., O'Brien, R. E., Kelly, S. T., Shilling, J. E., Moffet, R. C., Gilles, M. K., and Laskin, A.: Reactivity of liquid and semisolid secondary organic carbon with chloride and nitrate in atmospheric aerosols, The journal of physical chemistry. A, 119, 4498-4508, 10.1021/jp510336q, 2015a.
Wang, G. H., Zhang, R. Y., Gomez, M. E., Yang, L. X., Zamora, M. L., Hu, M., Lin, Y., Peng, J. F., Guo, S., Meng, J. J., Li, J. J., Cheng, C. L., Hu, T. F., Ren, Y. Q., Wang, Y. S., Gao, J., Cao, J. J., An, Z. S., Zhou, W. J., Li, G. H., Wang, J. Y., Tian, P. F., Marrero-Ortiz, W., Secrest, J., Du, Z. F., Zheng, J., Shang, D. J., Zeng, L. M., Shao, M., Wang, W. G., Huang, Y., Wang, Y., Zhu, Y. J., Li, Y. X., Hu, J. X., Pan, B., Cai, L., Cheng, Y. T., Ji, Y. M., Zhang, F., Rosenfeld, D., Liss, P. S., Duce, R. A., Kolb, C. E., and Molina, M. J.: Persistent sulfate formation from London Fog to Chinese haze, Proceedings Of the National Academy Of Sciences Of the United States Of America, 113, 13630-13635, 10.1073/pnas.1616540113, 2016.
Wang, J., Doussin, J. F., Perrier, S., Perraudin, E., Katrib, Y., Pangui, E., and Picquet-Varrault, B.: Design of a new multi-phase experimental simulation chamber for atmospheric photosmog, aerosol and cloud chemistry research, Atmospheric Measurement Techniques, 4, 2465-2494, 2011.
Wang, W. G., Li, K., Zhou, L., Ge, M. F., Hou, S. Q., Tong, S. R., Mu, Y. J., and Jia, L.: Evaluation and Application of Dual-Reactor Chamber for Studying Atmospheric Oxidation Processes and Mechanisms,

Acta Physico-Chimica Sinica, 31, 1251-1259, 2015b.
Wang, X., Liu, T., Bernard, F., Ding, X., Wen, S., Zhang, Y., Zhang, Z., He, Q., Lü, S., Chen, J., Saunders, S., and Yu, J.: Design and characterization of a smog chamber for studying gas-phase chemical mechanisms and aerosol formation, Atmospheric Measurement Techniques, 7, 301-313, 10.5194/amt-7-301-2014, 2014.
Warneke and C.: Comparison of daytime and nighttime oxidation of biogenic and anthropogenic VOCs along the New England coast in summer during New England Air Quality Study 2002, Journal of Geophysical Research Atmospheres, 109, D10309, 2004.
Wenger, J. C.: Chamber Studies on the Photolysis of Aldehydes Environmental, Dordrecht, 111-119, 2006.
White, S., Angove, D., Li, K. W., Campbell, I., Element, A., Halliburton, B., Lavrencic, S., Cameron, D., Jamie, I., and Azzi, M.: Development of a new smog chamber for studying the impact of different UV lamps on SAPRC chemical mechanism predictions and aerosol formation, Environmental Chemistry, 15, 171-182, 2018.
Wu, S., Lu, Z. F., Hao, J. M., Zhao, Z., Li, J. H., Hideto, T., Hiroaki, M., and Akio, Y.: Construction and characterization of an atmospheric simulation smog chamber, Adv Atmos Sci, 24, 250-258, 2007.
Zhang, Y., Sanchez, M. S., Douet, C., Wang, Y., Bateman, A. P., Gong, Z., Kuwata, M., Renbaum-Wolff, L., Sato, B. B., Liu, P. F., Bertram, A. K., Geiger, F. M., and Martin, S. T.: Changing shapes and implied viscosities of suspended submicron particles, Atmospheric Chemistry And Physics, 15, 7819-7829, 2015.
Zhang, Y., Chen, Y., Lei, Z., Olson, N. E., Riva, M., Koss, A. R., Zhang, Z., Gold, A., Jayne, J. T., Worsnop, D. R., Onasch, T. B., Kroll, J. H., Turpin, B. J., Ault, A. P., and Surratt, J. D.: Joint Impacts of Acidity and Viscosity on the Formation of Secondary Organic Aerosol from Isoprene Epoxydiols (IEPOX) in Phase Separated Particles, ACS Earth and Space Chemistry, 3, 2646-2658, 10.1021/acsearthspacechem.9b00209, 2019.
Zhang, Y., Chen, Y., Lambe, A. T., Olson, N. E., Lei, Z., Craig, R. L., Zhang, Z., Gold, A., Onasch, T. B., Jayne, J. T., Worsnop, D. R., Gaston, C. J., Thornton, J. A., Vizuete, W., Ault, A. P., and Surratt, J. D.: Effect of the Aerosol-Phase State on Secondary Organic Aerosol Formation from the Reactive Uptake of Isoprene-Derived Epoxydiols (IEPOX), Environmental Science & Technology Letters, 5, 167-174, 10.1021/acs.estlett.8b00044, 2018.
Zheng, J., Shi, X. W., Ma, Y., Ren, X. R., Jabbour, H., Diao, Y. W., Wang, W. W., Ge, Y. F., Zhang, Y. C., and Zhu, W. H.: Contribution of nitrous acid to the atmospheric oxidation capacity in an industrial zone in the Yangtze River Delta region of China, Atmospheric Chemistry And Physics, 20, 5457-5475, 2020.
Zhou, S., Hwang, B. C. H., Lakey, P. S. J., Zuend, A., Abbatt, J. P. D., and Shiraiwa, M.: Multiphase reactivity of polycyclic aromatic hydrocarbons is driven by phase separation and diffusion limitations, Proc Natl Acad Sci U S A, 116, 11658-11663, 10.1073/pnas.1902517116, 2019.
Zielinska, B., Sagebiel, J., Stockwell, W., McDonald, J., Seagrave, J., Wiesen, P., and Wirtz, K.: Investigation of Atmospheric Transformations of Diesel Emissions in the European Photoreactor (EUPHORE), Dordrecht, 279-284, 2006.
Ziemann, P. J. and Atkinson, R.: Kinetics, products, and mechanisms of secondary organic aerosol formation, Chemical Society reviews, 41, 6582-6605, 10.1039/c2cs35122f, 2012.